

Progresses in Experimental Study of N₂ Plasma Diagnostics by Optical Emission Spectroscopy

Hiroshi Akatsuka
Tokyo Institute of Technology,
Japan

1. Introduction

Nitrogen plasmas have been widely applied to material or electronic engineering, for example, metal-surface treatment for super-hard coating, preparation of innovative insulating layers, etc. For these processes, various plasma parameters are of great importance to control the characteristics of the prepared materials. From the engineering point of view, non-intrusive measurement method is desirable. Consequently, optical emission spectroscopy (OES) measurement is one of the best methods to examine various plasma parameters. In addition to applications, the nitrogen plasma plays an important role in many fundamental problems related to environmental issues. To understand the kinetics of radicals in the upper atmosphere or ionosphere including NO_x generation or ozone destruction, we should study the kinetics of the electronic or vibrational excited states of nitrogen discharge (Fridman, 2008; d'Agostino et al., 2008; Guerra & Loureiro, 1997).

In most of industrial applications or geophysical phenomena, the nitrogen plasma is in a state of non-equilibrium. Consequently, the gas temperature is much lower than the electron temperature. In order to estimate approximate value to the gas temperature, rotational temperature measurement is being frequently applied in practical researches and industries (Hrachová et al., 2002). Particularly, the spectrum of the second positive system (2PS), emitted as transitions from C ³Π_u state to B ³Π_g state, is easy to obtain its vibrational and rotational temperatures owing to its simple transition scheme. These temperatures are determined as best theoretical fitting parameters for the spectrum observed experimentally. Observation of this band is also easy from the experimental point of view (Phillips, 1976; Koike et al., 2004; Kobori et al., 2004; Yuji et al., 2007).

In the meanwhile, the first positive system (1PS), another band in the visible wavelength region, was difficult to analyze because of the complicated selection rule of the corresponding transition from B ³Π_g state to A ³Σ_u⁺ state. In order to obtain many experimental parameters as well as to understand the characteristics of non-equilibrium of each electronically excited state, quantitative measurement of 1PS of several vibrational levels is also significant for the understanding of nitrogen plasma (Sakamoto et al., 2006).

Another important parameter for the practical applications or for fundamental discussion of the nitrogen plasma is the dissociation degree, which is considered to be the one of the most

critical parameters for the processing. Many studies are being carried out both theoretically and experimentally on nitrogen dissociation in various discharge plasmas containing nitrogen gas. Experimentally, the most convenient method to measure the dissociation degree is the actinometry method based on optical emission spectroscopy (OES) measurement (Tatarova et al., 2005; Czerwicz et al., 2005). To deduce the dissociation degree of nitrogen molecules, we must know the ratio of the line intensity emitted from some excited states of atomic nitrogen to that from the excited actinometric molecule mixed into the plasma with its amount precisely controlled, for which argon has often been chosen. However, all of them severely overlap the 1PS band spectrum. Unless the dissociation degree is high enough to neglect the 1PS band intensity, precise evaluation of the dissociation degree seems almost impossible. If we calculate the 1PS band spectrum and subtract it from the observed emission spectrum, it is possible for us to extract the atomic nitrogen lines to apply the actinometry method by OES measurement.

Concerning the non-equilibrium of each band spectrum, it should be also remarked that the band spectra of molecular ions sometimes show their rotational temperatures different from those of neutral molecules. As for nitrogen ions, a number of papers reported that the first negative system (1NS), originated from $B\ ^2\Sigma_u^+$ state of N_2^+ ion, shows higher rotational temperature than that from neutral molecules (e.g., Huang et al., 2008).

On the other hand, it is also quite important to study reaction kinetics in nitrogen plasmas to understand quantitative amount of various excited species including reactive radicals. Many theoretical models have been proposed to describe the number densities of excited states in the plasmas. Excellent models involve simultaneous solvers of the Boltzmann equation to determine the electron energy distribution function (EEDF) and the vibrational distribution function (VDF) of nitrogen molecules in the electronic ground state. Consequently, we have found noteworthy characteristics of the number densities of excited species including dissociated atoms in plasmas as functions of plasma parameters such as electron density, reduced electric field, and electron temperature (Guerra et al., 2004; Shakhmatov & Lebedev, 2008).

From the viewpoints summarized above, we report our recent progress in spectroscopic analyses of 2PS, 1PS, and 1NS band spectra and actinometry measurement. We should also discuss a model to describe excitation kinetics in the nitrogen plasma. In section 2, the method to calculate the 2PS spectrum is described in detail. In section 3, a similar method to calculate 1PS spectrum is described. In section 4, we describe the similar fundamentals to analyze 1NS spectrum. In section 5, we concentrate on the actinometer measurement of dissociation degree of N_2 molecule by 1PS-subtraction, and discuss the dependence of the dissociation degree on the discharge conditions, particularly on the mixture ratio with rare gases. In section 6, we review a model to describe excitation kinetics in the nitrogen plasma. We also discuss dominant elementary processes to determine number densities of $B\ ^3\Pi_g$ or $C\ ^3\Pi_u$ states for the interpretation of spectroscopic data.

2. Spectrum of the N_2 Second Positive System (2PS)

The 2PS system corresponds to a transition between the electronic states $C\ ^3\Pi_u$ and $B\ ^3\Pi_g$. This band dominates the spectral region about 300 – 490 nm. We can find 2PS band in various nitrogen discharge or atmospheric gas discharge plasmas.

2.1 Theoretical background for spectral analysis of 2PS

First, let us consider the energy levels of upper and lower levels of the 2PS. Both states are the triplet system, which exhibits three sub-bands corresponding to the transitions ${}^3\Pi_0 - {}^3\Pi_0$, ${}^3\Pi_1 - {}^3\Pi_1$ and ${}^3\Pi_2 - {}^3\Pi_2$. Fortunately, the splitting is smaller than the separation of rotational lines. In the present study, we assume that the rotational lines remain unresolved, and consequently, we can justifiably neglect the spin splitting; the line strengths for the P, Q and R branches are combined (Phillips, 1976; Nunomura et al., 2006).

The energy of a N₂ molecule is given by a sum of its electronic E_e , vibrational $E_v(v)$ and rotational energies $E_r(v, J)$:

$$E(v, J) = E_e + E_v(v) + E_r(v, J), \quad (1)$$

where $E_v(v)$ and $E_r(v, J)$ are given by

$$E_v(v) = \omega_e \left(v + \frac{1}{2} \right) - \omega_e x_e \left(v + \frac{1}{2} \right)^2 + \dots, \quad (2)$$

$$E_r(v, J) = B_v J(J+1) - D_v J^2(J+1)^2 + \dots, \quad (3)$$

$$B_v = B_e - \alpha_e \left(v + \frac{1}{2} \right) + \dots, \quad (4)$$

$$D_v = D_e - \beta_e \left(v + \frac{1}{2} \right) + \dots. \quad (5)$$

Here, v and J are the vibrational and rotational quantum numbers, respectively. The coefficients in eqs. (2) – (5) are listed in Table 1. The energy of an emitted photon associated with an electronic transition from C ${}^3\Pi_u(v', J')$ to B ${}^3\Pi_g(v'', J'')$ is given by

$$E_{Bv'', J''}^{Cv', J'} = E_C(v', J') - E_B(v'', J''), \quad (6)$$

where $E_e(v, J)$ is the energy level of the electronic state e ($e = B$ or C) with vibrational quantum number v and rotational quantum number J , and $E_{Bv'', J''}^{Cv', J'}$ is the energy of the emitted photon. The corresponding frequency and wavelength is given by

$$\nu_{Bv'', J''}^{Cv', J'} = E_{Bv'', J''}^{Cv', J'} / h, \quad \lambda_{Bv'', J''}^{Cv', J'} = hc / E_{Bv'', J''}^{Cv', J'}, \quad (7)$$

where h and c are the Planck constant and the speed of light in vacuum, respectively. Since 2PS is an electric dipole transition, we apply the following selection rule:

| Electronic State | E_e [10 ⁴ cm ⁻¹] | ω_e [10 ³ cm ⁻¹] | $\omega_e x_e$ [10 ¹ cm ⁻¹] | B_e [cm ⁻¹] | α_e [10 ⁻² cm ⁻¹] |
|------------------|--|---|---|------------------------------|--|
| C ${}^3\Pi_u$ | 8.913 688 | 2.047 17 | 2.844 5 | 1.824 7 | 1.868 |
| B ${}^3\Pi_g$ | 5.961 935 | 1.733 39 | 1.412 2 | 1.637 4 | 1.791 |

Table 1. Coefficients of the N₂ 2PS.

$$\Delta J \equiv J' - J'' = 0, \pm 1, \quad (8)$$

except for $J' = 0 \rightarrow J'' = 0$. The values of ΔJ yield three branches: P, Q and R-branch, corresponding to $\Delta J = -1, 0$ and $+1$, respectively.

Basically, the nitrogen plasmas in our low-pressure (~ 1 Torr) steady-state discharge can be considered to be optically thin, at least for the 2PS band. This is because the order of electron density is 10^{13} cm^{-3} at most, and the number density of the lower level is considered to be low enough for us to neglect reabsorption.¹ Under the optically thin condition, the intensity of the spectrum is proportional to the population density of the upper level $N_C(v', J')$ and the transition probability $A_{Bv'', J''}^{Cv', J'}$:

$$I_{Bv'', J''}^{Cv', J'} \propto A_{Bv'', J''}^{Cv', J'} \cdot N_C(v', J'). \quad (9)$$

The population density of rotational levels is generally found to obey the Boltzmann distribution, at least for $C^3\Pi_u$ state, which we have confirmed for many 2PS spectra observed experimentally by theoretical fitting (Koike et al., 2004; Sakamoto et al., 2006; Yuji et al., 2007; Nunomura et al., 2006). On the other hand, the vibrational levels of $N_2 C^3\Pi_u$ state do not obey the Boltzmann distribution in general due to complicated kinetics to form vibrational levels, as later shown in section 6. We define the vibrational temperature T_V over several vibrational levels with the assumption that the levels are in the Boltzmann distribution. The population density is expressed as

$$N_C(v', J') = (2J' + 1) N_C(0, 0) \exp\left[-\frac{E_C(v', 0) - E_C(0, 0)}{kT_V}\right] \cdot \exp\left[-\frac{E_C(v', J') - E_C(v', 0)}{kT_R}\right], \quad (10)$$

where k is the Boltzmann constant. The transition probability $A_{Bv'', J''}^{Cv', J'}$ is given by

$$A_{Bv'', J''}^{Cv', J'} = \frac{64\pi^4 \left(\nu_{Bv'', J''}^{Cv', J'}\right)^3}{3hc^3 g_C} \cdot \frac{1}{2J' + 1} \sum_{jj''} |R_{jj''}|^2 \cdot q_{v'v''} S_{JJ''}, \quad (11)$$

where $\sum_{jj''} |R_{jj''}|^2$ is the transition moment and just a constant, g_C is the statistical weight of the $C^3\Pi_u$ state and also a constant, $q_{v'v''}$ is the Franck-Condon factor and $S_{JJ''}$ is the Hönl-London factor. Some of the Franck-Condon factors for small (v', v'') are listed in many textbooks, e.g., Ochkin, 2009. Meanwhile, we referred the Hönl-London factor $S_{JJ''}$ for P, Q, and R-branches to Phillips 1976, where the spin-splitting is neglected due to their smaller separation than the rotational lines, and the line strengths for the P, Q and R branches are combined. This approximation is allowed only when we treat the 2PS bands rotationally unresolved, which is exactly the case in the present analysis.

In actual spectrum measurement, the line spectrum is always broadened mainly due to a finite spectral resolution of an optical setup, where the line shape can be often approximated as Gaussian practically. When we introduce the spectral resolution as the full width of the half maximum (FWHM), the spectrum is finally written as follows:

¹ It should be noted that some pulse-discharge plasmas with high electron density can be optically thick even for 2PS transition.

$$I(\lambda) = \sum_{v', v'', J', J''} I_{Bv'', J''}^{Cv', J'} \exp \left[- \left(\frac{\lambda - \lambda_{Bv'', J''}^{Cv', J'}}{\Delta\lambda} \right)^2 \right], \quad (12)$$

$$\Delta\lambda = \frac{\text{FWHM}}{2\sqrt{\ln 2}}, \quad (13)$$

where λ is the wavelength of observed spectrum.

Figure 1 shows the spectrum of the N₂ 2PS for $\Delta v = v' - v'' = -2$, calculated by eqs. (1) - (13). The 2PS spectrum has sharp band heads at the longer wavelength side and long tails at the shorter wavelength side. Since the 2PS spectrum has such a distinct feature, a fit of the observed spectrum to the calculated one yields T_V and T_R as best fitting parameters. Figure 2 is an example of comparisons between spectra calculated theoretically and measured experimentally for microwave discharge nitrogen plasma with its pressure 1 Torr.

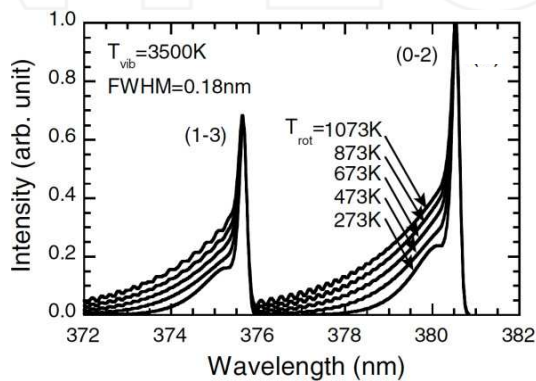


Fig. 1. Calculated spectrum of the N₂ 2PS of $\Delta v = -2$, assuming $T_V = 3500$ K and FWHM = 0.18 nm (Nunomura et al., 2006).

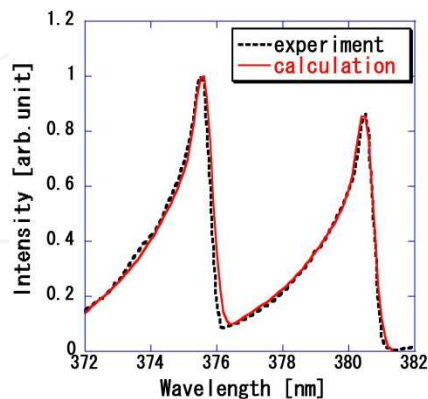


Fig. 2. Example of comparison between 2PS spectra calculated theoretically and measured experimentally, assuming $T_V = 0.90$ eV and $T_R = 0.15$ eV (Sakamoto et al., 2006, 2007).

2.2 Examples of 2PS spectra measured experimentally and discussion on the vibrational and rotational temperatures

In our laboratory, we have been examining spectroscopic characteristics of microwave discharge nitrogen plasma. Figure 3 shows the schematic diagram of our experimental setup. We generate a nitrogen plasma, using a rectangular waveguide with a cavity and a quartz tube, one end of which was inserted into a vacuum chamber. The quartz tube (i.d. 26 mm) was aligned in the direction of the electric field of the waveguide. The microwave frequency was 2.45 GHz and the output power was set at 600 W. The discharge pressure was 0.5 – 5.0 Torr. The gas feed rate was set at approximately 100 – 300 ml/min using a flow controller. Further details of the detection system are specified elsewhere (Sakamoto et al., 2006, 2007).

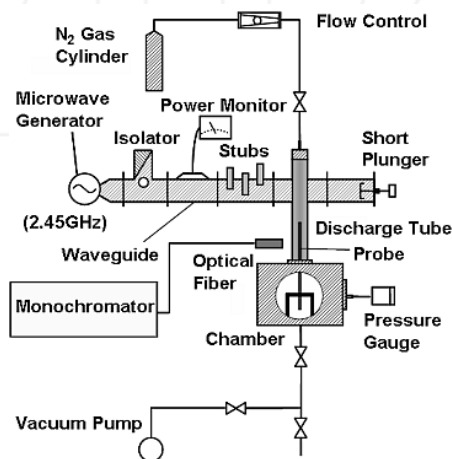


Fig. 3. Schematic diagram of microwave discharge apparatus and measurement system.

Figures 4 (a) and (b) shows T_R and T_V of the $N_2 C^3\Pi_u$ state, respectively. T_R decreased as the plasma flowed to the downstream direction, i.e., to larger z . It is considered that this result is

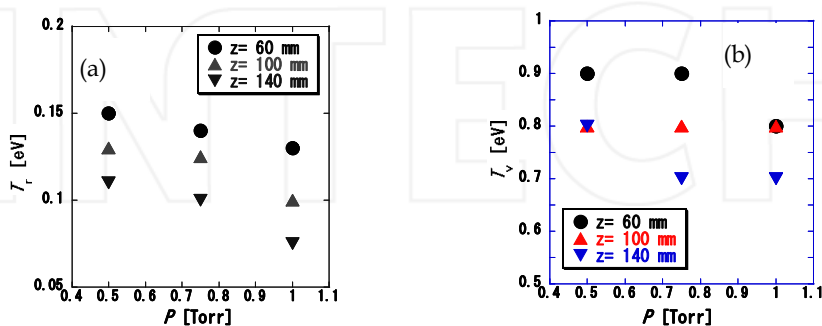


Fig. 4. (a) Rotational and (b) vibrational temperatures of $C^3\Pi_u$ state of N_2 plasma measured experimentally, generated in the apparatus schematically shown in Fig. 3 ($\Delta v = -2$, $v' = 0, 1$) (Sakamoto et al., 2007).

obtained because of the cooling of neutral component of discharge species, since it is mostly heated at the discharge position $z = 0$. Consequently, the variation in the rotational temperature is considered to be useful for the analysis of macroscopic thermal structure of nitrogen plasma, which is mostly determined by the temperature of neutral particles (Nunomura et al., 2006; Yuji et al., 2007, 2008).

Concerning the vibrational temperature, there is some experimental error (± 0.05 eV) that is primarily caused by the fitting procedure. The vibrational temperature is much higher than the rotational temperature, since the vibrational kinetics is considerably determined by the electron impact excitation. The vibrational temperature decreased with increasing discharge pressure. It is considered that the collisional relaxation of molecules proceeds rapidly at higher discharge pressure (Sakamoto et al., 2006, 2007).

3. Spectrum of the N₂ First Positive System (1PS)

This transition appears between the electronic states B ³Π_g and A ³Σ_u⁺. Emission spectrum of 1PS is found in the wide wavelength region from 500 nm to 1100 nm.

3.1 Theoretical background for spectral analysis of 1PS

First, let us consider the energy levels of B ³Π_g state, for which every rotational level K is subdivided into three sublevels with their quantum numbers J corresponding to $J = K + 1$, K , and $K - 1$. We must treat the energy level of the B ³Π_g state more precisely for 1PS than for 2PS. We write subscript numbers 1, 2, and 3 corresponding to $J = K + 1$, K , and $K - 1$, respectively, in the following equations. The rotational term values are

$$F_1(J) = B_v \left[J(J+1) - \sqrt{Z_1} - 2Z_2 \right] - D_v \left(J - \frac{1}{2} \right)^4, \quad (14)$$

$$F_2(J) = B_v \left[J(J+1) + 4Z_2 \right] - D_v \left(J + \frac{1}{2} \right)^4, \quad (15)$$

$$F_3(J) = B_v \left[J(J+1) + \sqrt{Z_1} - 2Z_2 \right] - D_v \left(J + \frac{3}{2} \right)^4, \quad (16)$$

with

$$Z_1 = Y(Y-4) + \frac{4}{3} + 4J(J+1), \quad (17)$$

$$Z_2 = \frac{1}{3Z_1} \left[Y(Y-1) - \frac{4}{9} - 2J(J+1) \right], \quad (18)$$

where

$$Y = A_v/B_v, \quad (19)$$

and A_v is the spin-orbit interaction parameter

$$A_v = 42.286 - 0.068 \left(v + \frac{1}{2} \right) - 2.5 \times 10^{-3} \left(v + \frac{1}{2} \right)^2 - 2.6 \times 10^{-4} \left(v + \frac{1}{2} \right)^3 \quad [\text{cm}^{-1}], \quad (20)$$

and B_v and D_v are defined by equations (4) and (5), respectively. For $B \ ^3\Pi_g$ state, $D_e = 5.52 \times 10^{-6} \text{ cm}^{-1}$, and $\beta_e = 9 \times 10^{-8} \text{ cm}^{-1}$.

Next, for the electronic state $A \ ^3\Sigma_u^+$, the rotational term values are

$$F_1(K) = B_v K(K+1) - D_v K^2(K+1)^2 + \frac{6w(K+1)}{2K+3} - x(K+1), \quad (21)$$

$$F_2(K) = B_v K(K+1) - D_v K^2(K+1)^2, \quad (22)$$

$$F_3(K) = B_v K(K+1) - D_v K^2(K+1)^2 + \frac{6w(K+1)}{2K-1} - xK, \quad (23)$$

where $w = 0.443 \text{ cm}^{-1}$, $x = 3 \times 10^{-3} \text{ cm}^{-1}$, $B_e = 1.4539 \text{ cm}^{-1}$, $\alpha_e = 0.0175 \text{ cm}^{-1}$, $D_e = 5.46 \times 10^{-6} \text{ cm}^{-1}$, and $\beta_e = 1.1 \times 10^{-7} \text{ cm}^{-1}$ (Sakamoto et al., 2006, 2007).

Since $^{14}\text{N}_2$ is a homonuclear molecule, we must consider the selection rule with respect to the symmetry (s) and anti-symmetry (a). Namely, the transitions $s \leftrightarrow s$ and $a \leftrightarrow a$ are allowed. We must keep the statistical weights for the symmetric and anti-symmetric levels are in the ratio 2 : 1 since $^{14}\text{N}_2$ is with nuclear spin $I = 1$ for each N. When we apply these regulations to 1PS transition, we have the selection rules as schematically shown in Fig. 5. For example, the transition P_{33} belongs to an $a \leftrightarrow a$ transition and Q_{33} to an $s \leftrightarrow s$ transition.

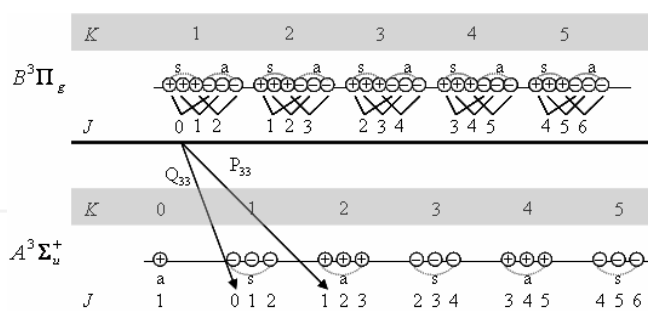


Fig. 5. Schematic diagram to illustrate the selection rule with respect to the symmetry (s) and anti-symmetry (a) of 1PS. The transitions $s \leftrightarrow s$ and $a \leftrightarrow a$ are allowed (Ichikawa et al., 2010).

During the course of our spectroscopic study of microwave discharge nitrogen plasma, we found that neither the Hund's coupling case (a) nor (b) holds for the 1PS transition for general discharge nitrogen plasmas with a high gas temperature owing to the large energy gap between highly excited rotational levels. We proposed the transition scheme in Fig. 6, where we consider 27 all the allowed transitions that satisfy the selection rule $\Delta l = 0, \pm 1$ for variation in the rotational quantum number. The Franck-Condon and the Hönl-London factors used are specified elsewhere (Sakamoto et al., 2007).

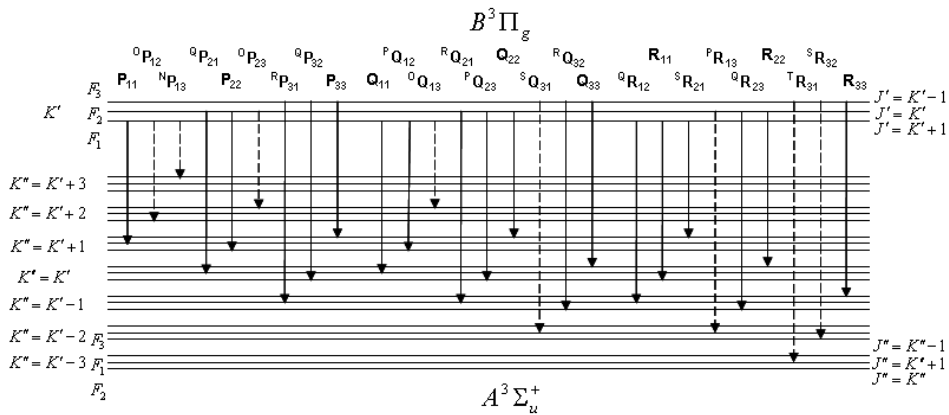


Fig. 6. Transition scheme of N₂ 1PS. The filled lines denote the transitions given by Hund's coupling case (b), whereas the broken lines are those newly included in our study (Sakamoto et al., 2007; Ichikawa et al., 2010).

Figure 7 is an example of comparison between the 1PS spectrum calculated on the basis of the scheme indicated in Fig. 6 and the one measured experimentally from 635 nm to 655 nm. Obviously, the agreement is excellent. Small maxima around 641 and 648 nm are well reproduced theoretically and the agreement with the experimental results is satisfactory. In the meanwhile, we could not reproduce the maxima around 641 and 648 nm in Hund's (b) scheme, which did not agree with the experimental results well. These small maxima may be, in some sense, considered to be minor, and indeed, we can determine the rotational or vibrational temperatures as best fitting parameters. However, if we would like to reproduce the whole 1PS spectrum to find other line spectra overlapped in the wavelength region of 1PS, we should trace the shape of spectrum as precise as possible. Particularly, as shown in section 5, to extract lines of atomic nitrogen, we should calculate the spectra precisely. For this reason, the rigorous transition scheme should be reflected on the theoretical calculation of 1PS spectrum.

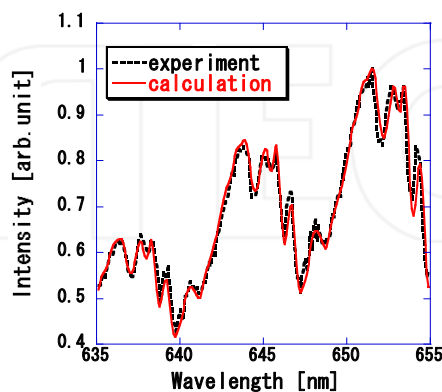


Fig. 7. Example of comparison between 1PS ($\Delta v = 3$) spectra calculated theoretically and measured experimentally, assuming $T_V = 0.65$ eV and $T_R = 0.15$ eV (Sakamoto et al., 2007).

3.2 Experimental results and discussion on vibrational and rotational temperatures determined from 1PS spectrum in comparison with those from 2PS spectrum

Figures 8(a) and 8(b) show the rotational and vibrational temperatures, respectively, determined from the 1PS spectrum observed in the same discharge apparatus that is schematically shown in Fig. 3 and under the same discharge conditions when we observed the temperatures shown in Figs. 4. Figures 8(a) and 4(a) indicate that the rotational temperatures of both 1PS and 2PS are not so different from each other for the discharge pressure 0.5 – 1.0 Torr, both of which can be considered as approximate value to the gas translational temperature. The rotational temperature of 1PS also becomes lower as the plasma flows toward the downstream direction, since the collisional relaxation becomes essential. Particularly, when the discharge pressure is 1.0 Torr, the rotational temperatures both of 1PS and of 2PS are almost the same throughout the observed domain over the microwave discharge. The pressure as high as 1 Torr can enhance the collisional relaxation, and in consequence, both rotational temperatures are considered to agree very well with each other. Basically, the rotational constant B_e of nitrogen molecules is very small not only for the ground state $X\ ^1\Sigma_g^+$ but also for excited states $B\ ^3\Pi_g$, $C\ ^3\Pi_u$, etc. Therefore, the rotationally excited levels can frequently exchange kinetic energy with translational motion of neutral nitrogen molecules. Consequently, it is considered that the energy distribution of rotational levels is almost equilibrated with that of translational motion through a couple of collisions.

On the other hand, the vibrational temperature of 1PS is significantly lower than that of 2PS, as Figs. 8(b) and 4(b) indicate. However, the dependence on the discharge pressure is qualitatively similar, i.e., the vibrational temperature tends to decrease as the discharge pressure increases. This can also be attributed to the frequent collisional relaxation with neutral molecules. The discrepancy on vibrational temperatures between 1PS and 2PS can be explained by the dominant molecular processes for the excitation and de-excitation of the upper state of 1PS and 2PS, that is, $B\ ^3\Pi_g$ and $C\ ^3\Pi_u$. This will be discussed in section 6 in terms of elementary processes in the nitrogen plasma with low discharge pressure.

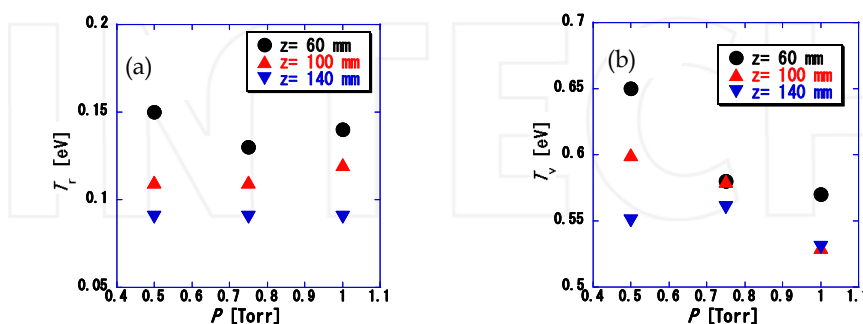


Fig. 8. (a) Rotational and (b) vibrational temperatures of $B\ ^3\Pi_g$ state of N_2 plasma measured experimentally, generated in the apparatus schematically shown in Fig. 3 ($\Delta v = 3$, $v' = 7, 8, 9$) (Sakamoto et al., 2007).

4. Spectrum of the N₂⁺ First Negative System (1NS)

1NS is originated from the transition between the excited sates of molecular ion N₂⁺ B ²Σ_u⁺ and the ground state of ion N₂⁺ X ²Σ_g⁺. It is found near UV through shorter visible wavelength range, from 320 to 450 nm, which almost overlaps the 2PS spectrum.

4.1 Theoretical background for spectral analysis of 1NS

Since 1NS is a ²Σ_u⁺ → ²Σ_g⁺ transition, the coupling scheme is given by the Hund's (b) coupling case. Although 1NS can be basically approximated by a P- and an R-branches, this transition has a fine structure owing to spin multiplicity. However, the structure is sufficiently fine to be neglected in general. Then, the numbering of the branches should be dependent on K which appears in the Hund's (b), not on J. Consequently, the rotational energy should be described not with equation (3), but by the following equations:

$$E_1(K) = B_v K(K+1) + \frac{1}{2} \gamma K, \quad \left(J = K + \frac{1}{2} \right) \text{ (P}_1, \text{R}_1 \text{ branches)}, \quad (24)$$

$$E_2(K) = B_v K(K+1) - \frac{1}{2} \gamma (K+1), \quad \left(J = K - \frac{1}{2} \right) \text{ (P}_2, \text{R}_2 \text{ branches)}, \quad (25)$$

where γ is the spin splitting constant. The rotational term is split into two components as eqs. (24) - (25) for two possible values of the quantum number J, where J is the absolute value of the vector J that is defined as the vector-like summation of $J = K + S$. In the present scheme $S = |S| = 1/2$. Each line is split into three components corresponding $\Delta J = J' - J'' = -1, 0, \text{ and } +1$. This indicates that the essential transition structure of 1NS band spectrum is decomposed into the scheme as depicted in Fig. 9. However, the components with $\Delta J = 0$ (P_{Q12} and R_{Q21}) are weak enough to be neglected. In consequence, the 1NS spectrum can be satisfactorily reproduced by the summation of four components, P₁, P₂, R₁, and R₂, as shown in Fig. 9 (Bingel, 1967). Concerning Franck-Condon and Hönl-London factors of 1NS transition, we adopted Ochkin 2009, which is a practical and useful textbook published recently, and also briefly summarized other transition schemes (Ochkin, 2009).

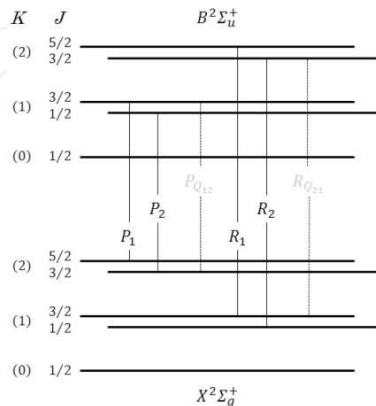


Fig. 9. Transition scheme of N₂⁺ 1NS. Those indicated in thin lines are negligibly weak.

The band spectrum of 1NS $\Delta v = -1$, which has the strongest intensity in 1NS, is entirely overlapped with that of 2PS. Therefore, 1NS must be fitted simultaneously with 2PS. The intensity of 1NS in comparison with that of 2PS, of course, depends on the discharge conditions. In common low-temperature nitrogen discharge plasmas, the ionization degree is not so high, and consequently, the intensity of 1NS is weaker than that of 2PS. We chose the wavelength region from 410 to 430 nm ($\Delta v = -1$) where both intensities were almost comparable in the nitrogen plasma generated in our apparatus shown in Fig. 3. First, we determined the T_V and T_R of 2PS for $\Delta v = -2$ by the procedure in section 2 for the wavelength region from 372 to 382 nm. After that, we determine T_V and T_R of 1NS by fitting procedure for the spectrum from 410 to 430 nm with the previously fixed $T_V(2PS)$ and $T_R(2PS)$ for the band $\Delta v = -4$ of 2PS.

Figure 10 shows an example of comparison between the spectrum calculated theoretically and the one measured experimentally. We found a good agreement for the longer wavelength region in Fig. 10, i.e., from 421 to 428 nm, where there exist $(v', v'') = (0, 1), (1, 2)$ bands of 1NS and $(1, 5)$ of 2PS. We found that the bands $\Delta v = -4$ of 2PS for the wavelength region shorter than 421 nm cannot be calculated precisely by the method described in section 2, particularly in the tail region where the R-branch becomes predominant. The spectrum of 2PS bands with $(2, 6)$ or higher vibrational quantum numbers requires some modification. However, in the present analysis, the objective is to determine T_V and T_R of 1NS, which is practically carried out for the wavelength region from 421 to 428 nm precisely. The band heads of 1NS are much more sharp than that of 2PS, which allows us to determine T_V with satisfactory precision. On the other hand, $(1, 2)$ band of 1NS is rather isolated, and in consequence, T_R can be determined satisfactorily (Kawano et al., 2011).

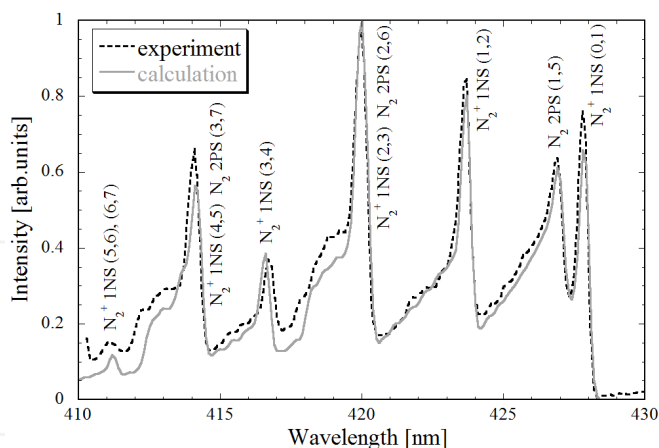


Fig. 10. Example of comparison between the spectrum of 1NS and 2PS calculated theoretically and the one observed experimentally (Kawano et al., 2011).

4.2 Results and discussion on difference in T_V and T_R between 1NS and 2PS

Figures 11(a) and 11(b) show the rotational and vibrational temperatures, respectively, determined from the 1NS spectrum observed in the same discharge apparatus schematically

shown in Fig. 3 under the same discharge conditions as in Figs. 4 and 8, except the discharge pressure is fixed at 1 Torr. Figure 11(a) indicates that the rotational temperature of $N_2^+ B^2\Sigma_u^+$ ion ranges from 0.14 – 0.35 eV, which is about 1.5 times higher than that of neutral $N_2 C^3\Pi_u$ determined from the OES of 2PS, 0.08 – 0.18 eV. It is also found that T_R of $N_2^+ B^2\Sigma_u^+$ ion also decreases as the plasma flows to the downstream direction.

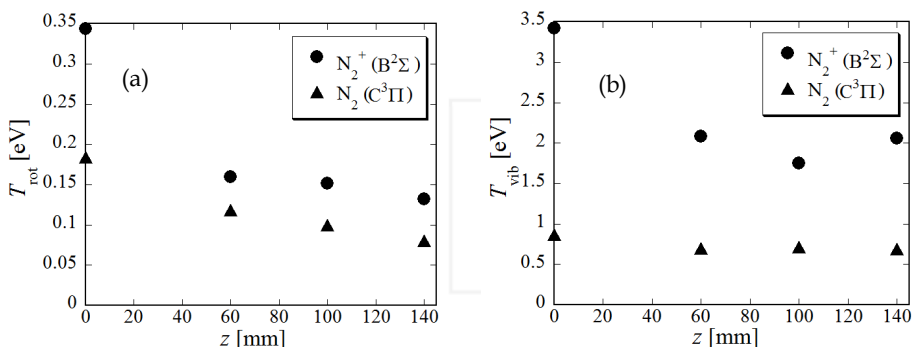


Fig. 11. (a) Rotational and (b) vibrational temperatures of $N_2^+ B^2\Sigma_u^+$ state of the plasma generated in the apparatus schematically shown in Fig. 3 (Kawano et al., 2011).

Basically, the rotational motion of the molecular species in the plasma is considered to be an approximate value to the gas translational temperature, which is the case for $N_2 C^3\Pi_u$ and $B^2\Sigma_u^+$ states as already shown in sections 2 and 3. However, the rotational temperature of 1NS is higher than those of 1PS and 2PS, and consequently, it does not correspond to the translational temperature of neutral molecules. Similar results are reported on T_R of 1NS of low-pressure discharge nitrogen plasmas (Huang et al., 2008). These experimental results possibly indicate that the dominant population process of excited states $B^2\Sigma_u^+$ of N_2^+ is not the direct excitation from the ground state of neutral N_2 molecule, and not from excited states of neutral molecular state, either. Otherwise, the rotational energy distribution of $N_2^+ B^2\Sigma_u^+$ should become almost the same with the initial state of the molecule.

One possible reason for the higher T_R of 1NS is that the predominant population process of $B^2\Sigma_u^+$ of N_2^+ ion is the electron impact excitation from the ground state $X^2\Sigma_g^+$ of N_2^+ ion, not from any state of neutral molecules. Then, the rotational energy distribution of $B^2\Sigma_u^+$ of N_2^+ should be close to that of the ground state $X^2\Sigma_g^+$ of N_2^+ ion. It is also noteworthy that T_V of 1NS is also about twice as high as that of 2PS as in Fig. 11(b). Further discussion is necessary to conclude the reason for the higher rotational temperature of 1NS.

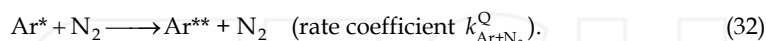
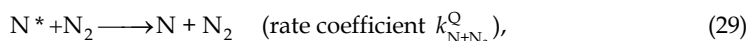
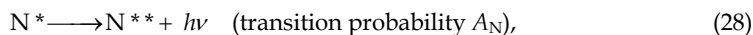
5. Measurement of dissociation degree of N_2 molecule in the nitrogen plasma by actinometry method with the help of 1PS subtraction

As we described in the introduction, one of the most important parameters to control the nitrogen plasma processes in industrial applications is the density of nitrogen atoms, or the dissociation degree of the nitrogen molecules in the discharge plasma. The most convenient and practical method of its measurement is the actinometry method. To do so, however, we must extract emission lines of atomic nitrogen, by the subtraction of 1PS band spectrum. In

this section, we describe the actinometry method with the help of 1PS subtraction to measure the dissociation degree of nitrogen (Ichikawa et al., 2010). We also experimentally examined the effect on the nitrogen dissociation degree of admixture of rare gases.

5.1 Basic principle of actinometry measurement for about 1 Torr discharge

In the general actinometer measurement of density of nitrogen atoms in the nitrogen plasma, we almost always choose argon as an actinometer. As actinometric signals, we generally choose the line intensities of $\lambda = 746.83$ nm for N I [3p $^4S^o$ (12.00 eV) \rightarrow 3s $^4P_{5/2}$], and $\lambda = 811.53$ nm for Ar I [2p₉ (i.e., 4p[5/2], 13.07 eV) \rightarrow 1s₅ (i.e., 4s[3/2]^o)]. In our study, we treat the N₂-rare gas mixture plasmas to examine the dissociation degree that must depend on the gas mixture ratio. In this subsection, we describe the basic principle of actinometry including atomic and molecular processes of the N₂-gas mixture discharge plasmas, which was applied to N₂-O₂ mixed discharge (Ichikawa et al., 2010). Regarding the population and depopulation of these states, we must consider the following reactions due to collisional relaxation by the ground-state molecules of N₂ for about a 1-Torr discharge to deduce the number density of nitrogen atoms.



For these transitions in the present discharge pressure range, the spectrum intensity ratio becomes

$$\frac{I_N}{I_{Ar}} = \frac{A_N}{A_{Ar}} \cdot \frac{\sum A_{Ar} + k_{Ar+N_2}^Q [N_2]}{\sum A_N + k_{N+N_2}^Q [N_2]} \cdot \frac{k_{M+e}^{\text{dir}} [N]}{k_{Ar}^{\text{exc}} [Ar]} \cdot \frac{\lambda_{Ar}}{\lambda_N} \cdot \frac{C(\lambda_N)}{C(\lambda_{Ar})}, \quad (33)$$

where [M] is the number density of species M, k^Q is the rate coefficient of the quenching reaction of the excited states at the line emission of the present OES measurement with their subscripts denoting the reactions [eqs. (29) and (32)], k^{dir} is that of direct electron impact excitation from the atomic ground state of N to produce the corresponding OES level [eq. (26)], k^{exc} is that for Ar [eq. (30)], λ is the wavelength of the transitions given by eqs. (28) and (31), A is the atomic transition probability of the corresponding transition, and $C(\lambda)$ is the detection

coefficient of the spectrometric system for the wavelength λ . If we add oxygen, rare gas or other dilution gas into nitrogen, we must consider the quenching effect of excited species by the admixture gas and modify eq. (33). We summarized the transition probabilities and rate coefficients required to eqs. (26) – (33) elsewhere in Ichikawa et al., 2010.

In the present analysis, the EEDF is determined by solving the Boltzmann equation as a function of the reduced electric field E/N so that the electron mean energy equals 3/2 times the electron temperature experimentally measured by the probe. The Boltzmann equation is simultaneously solved with the master equations for the vibrational distribution function (VDF) of the N₂ X ¹Σ_g⁺ state, since the EEDF of N₂-based plasma is strongly affected by the VDF of N₂ molecules owing to superelastic collisions with vibrationally excited N₂ molecules. A more detailed account of obtaining the EEDF is given in the next section.

Strictly speaking, the actinometry levels are also generated by the radiative decay of their upper levels, in addition to eq. (26), which is referred to as cascade processes. These processes are generally negligible for actinometry measurement in the present microwave discharge plasmas, which are categorized into ionizing plasmas. Further discussion was described elsewhere (Ichikawa et al., 2010).

5.2 Subtraction of 1PS-band spectrum as background signal to extract atomic nitrogen lines, and the lower limit of number density of nitrogen atoms

As we already showed in Fig. 7, we demonstrated theoretical fitting of 1PS as functions of vibrational and rotational temperatures for the transition series $\Delta v = v' - v'' = 3$. In order to extract the lines emitted from excited nitrogen atoms, we must calculate the 1PS spectrum with $\Delta v = v' - v'' = 2$, which can be done by the same procedure. After we experimentally measure the 1PS spectrum of the vibrational quantum numbers $\Delta v = v' - v'' = 2$ in the wavelength region of 730 – 760 nm, we determine T_v and T_r by the numerical fitting method. We consider that an argon line with a large peak appears at 750.4 nm. Consequently, we fit the spectrum excluding the wavelength region of 750 – 752 nm. Then, after we subtract the overall 1PS spectrum calculated as a background signal from the observed spectrum, we obtain the line of the excited nitrogen atom at 746.83 nm.

Figure 12(a) shows an example of fitting the 1PS band spectrum experimentally observed in the wavelength region of 730 – 760 nm with the one calculated theoretically, and Fig. 12(b) shows the result of subtraction, which indicates the successful extraction of atomic nitrogen line spectra, not only at 746.83 nm but also at 744.23 and 742.36 nm, which corresponds to the transitions $3p\ ^4S_{3/2} \rightarrow 3s\ ^4P_{5/2, 3/2, 1/2}$, respectively. The simultaneous extraction of these three lines indicates that the present method is reliable and that the contamination by other lines can be neglected with respect to other excited states of nitrogen and argon species. The line at 746.83 nm has the largest intensity among the three lines, and we chose it for the actinometry measurement. Here, we discuss the lower limit of the number density of nitrogen atoms that measured by the present method. Figure 12(b) is a typical example, which corresponds to a density of nitrogen atoms of $1.4 \times 10^{12}\text{ cm}^{-3}$, whereas the fluctuation of the baseline is about 1/20 times the peak height of the actinometry signal. The subtracted baseline illustrated in Fig. 12(b) is common to almost all the discharge conditions throughout the present experiments. As a result, the lower limit of the number density of nitrogen atoms is considered to be about $< 7 \times 10^{10}\text{ cm}^{-3}$ (Ichikawa et al., 2010).

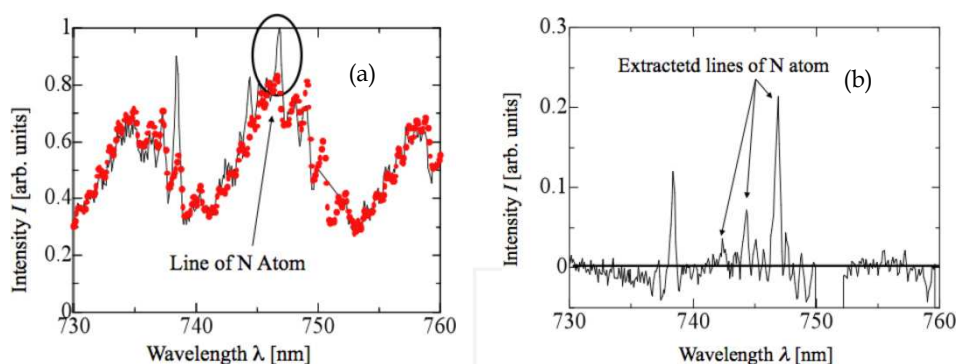


Fig. 12. (a) Schematic diagram of the spectrum fitting of N_2 -1PS band spectrum and (b) the extracted lines of nitrogen atom. (a) Line – experimentally measured spectrum, dots – calculated spectrum by our method. We did not plot the experimental results in the wavelength region 750 – 752 nm since an Ar atomic line appears in this position with a large intensity (Ichikawa et al., 2010).

5.3 Results and discussion of actinometry measurement of dissociation degree of nitrogen molecule in N_2 -rare gas mixed microwave discharge plasma

In this study, we define the dissociation degree $D(N)$ of nitrogen as follows:

$$D(N) = [N] / (2[N_2]), \quad (34)$$

where $[X]$ is the number density of species X . The density $[N_2]$ is calculated from the discharge partial pressure and gas temperature, with the assumption that the number densities of any excited species are negligibly smaller than that of the ground state.

We experimentally examined the dependence of the dissociation degree of nitrogen on the mixture ratio of O_2 (Ichikawa et al., 2010) and various rare gas species (Kuwano et al., 2009). Here, we concentrate on rare-gas admixture. First, we examined the electron temperature and density by a Langmuir Double probe, as function of the gas mixture ratio. The admixture of lighter rare-gas species increases the electron temperature, since the lighter rare-gas species have higher ionization potential. On the other hand, the heavier rare-gas species have lower ionization potential, and consequently, the electron temperature can become lower and the electron density increases with increasing the volumetric ratio of heavier rare-gas species.

Figure 13 shows the measured dissociation degree plotted against the rare gas mixture ratio for the microwave discharge N_2 -rare gas plasma. When helium is mixed into the nitrogen plasma, we found a small increase in the nitrogen dissociation degree. This can be explained by an increase in the electron temperature by the helium admixture. On the other hand, when the argon or krypton with low-ionization energy was mixed into the nitrogen plasma, we found lowering of electron temperature and resultant reduction in the nitrogen dissociation degree. For these three kinds of rare gases, the variation in their dissociation degree is reasonable since it corresponds to the variation in the electron temperature (Kuwano et al., 2009).

Figure 13, however, shows that the neon admixture markedly enhances the nitrogen dissociation degree. This tendency was found even at considerable downstream positions like $z = 140$ mm. We now consider that the spectroscopic contamination of Ne I 747.24 nm into N I 746.83 nm is negligible owing to sufficient resolution of experimental setup. Some nitrogen plasma process may be conducted several hundred times faster than the conventional processes with neon admixture. We now consider that one of the possible mechanisms is that the energy-transfer collision between the metastable neon (16.62 or 16.72 eV) and nitrogen molecules, which makes it excited to the dissociation curve. Further discussion and cross-examination by other experimental methods are necessary to understand the dissociation of nitrogen molecules by neon admixture (Akatsuka et al., 2010).

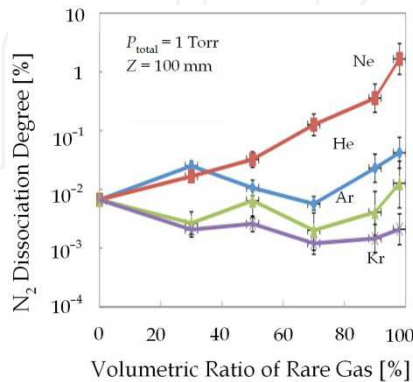


Fig. 13. Dissociation degree of nitrogen molecule plotted against N₂: rare-gas mixture ratio.

6. Numerical modelling of excitation kinetics in the N₂ plasma

Numerical studies on number densities of various excited states in the N₂ plasma have eagerly been carried out all over the world (Guerra et al., 2004; Shakhmatov & Lebedev, 2008). We also make a numerical code to calculate number densities as functions of the following parameters: gas temperature T_g , electron density N_e , total discharge pressure P , and reduced electric field E/N as a rather simplified model (Akatsuka et al., 2008; Ichikawa et al., 2010).

First, we assume that the geometry is axially symmetric and neglect the z -dependence. Concerning the density $[A]$ of species A , we have the following partial differential equation:

$$\frac{\partial [A]}{\partial t} = -\nu_w \cdot [A] + G, \quad (35)$$

where ν_w is the particle loss frequency due to wall collision or diffusion, and G is the net particle generation or loss due to volumetric reactions. We discuss the number densities of N₂(X ¹Σ_g⁺), N₂(A ³Σ_u⁺), N₂(B ³Π_g), N₂(C ³Π_u), N₂(a ¹Π_g), N₂(a' ¹Σ_u⁻), N₂⁺, N₄⁺, N(2p ⁴S_o), and e⁻. The cross sections, rate coefficients, or any required atomic and molecular data required in this section are summarized elsewhere in Ichikawa et al., 2010.

6.1 The Boltzmann equation

In order to calculate the various rate coefficients to solve eq. (35) as well as to evaluate the actinometry signal in the present experiments using eq. (33), we need the electron energy

probabilistic function (EPPF) in the discharge plasma, and consequently, we must solve the Boltzmann equation to describe the EPPF. To analyze cw discharge, the EPPF may be treated by a two-term approximation owing to the sufficiently small anisotropy. Consequently, the Boltzmann equation for the isotropic component of the EPPF $f_0(\varepsilon)$ is formulated as follows (Sakamoto et al., 2007; Mizuochi et al., 2010):

$$-\frac{d}{d\varepsilon} \left\{ \frac{1}{3} \left(\frac{E}{N} \right)^2 \frac{\varepsilon}{\sigma_c(\varepsilon)} \frac{df_0(\varepsilon)}{d\varepsilon} + \frac{2m_e}{M} \varepsilon^2 \sigma_c(\varepsilon) \left[f_0(\varepsilon) + \frac{kT_g}{e} \frac{df_0(\varepsilon)}{d\varepsilon} \right] \right\} + \sum_l \varepsilon \frac{N_l}{N} \sigma_l^{\text{si}}(\varepsilon) f_0(\varepsilon) - \sum_l \left(\varepsilon + \varepsilon_l^{\text{si}} \right) \frac{N_l}{N} \sigma_l^{\text{si}} \left(\varepsilon + \varepsilon_l^{\text{si}} \right) f_0 \left(\varepsilon + \varepsilon_l^{\text{si}} \right) = 0, \quad (36)$$

where e is the elementary charge, ε is the electron energy, σ_c is the momentum transfer cross section, σ_l^{si} is the l th inelastic collision cross section with the energy change of $\varepsilon_l^{\text{si}}$, m_e is the electron mass, M denotes the molecular mass of the elastic collision partner of the electron, and N_l is the number density of the l th inelastic collision partner. Table 2 summarizes the inelastic collisions included in eq. (36), where the EPPF $f_0(\varepsilon)$ is normalized as follows:

$$\int_0^\infty f_0(\varepsilon) \varepsilon^{1/2} d\varepsilon = 1. \quad (37)$$

| Inelastic Collisions | | |
|---------------------------------|---|---|
| $e^- + \text{N}_2(\text{X})$ | $\rightarrow e^- + \text{N}_2(\text{Y})$ | (Y = A ³ Σ _u ⁺ , B ³ Π _g , C ³ Π _u , a' ¹ Σ _u ⁺ , a ¹ Π _g , w ¹ Δ _u , B' ³ Σ _u ⁺ , W ³ Δ _u) |
| $e^- + \text{N}_2(\text{X})$ | $\rightarrow e^- + e^- + \text{N}_2^+$ | |
| $e^- + \text{N}_2(\text{X}, v)$ | $\leftrightarrow e^- + \text{N}_2(\text{X}, w)$ | (v, w = 0–8) |

Table 2. List of inelastic collisions included in the collision term in eq. (36).

6.2 Vibrational distribution function (VDF) of N₂ X¹Σ_g⁺ state

We must solve the Boltzmann equation [eq. (36)] simultaneously with the master equations to describe the VDF of the ground state of the nitrogen molecule. We consider the elementary processes shown in Table 3. We treat N plasmas with a very low dissociation degree of its order about 10^{−3}, and consequently, we neglect the V-T relaxation by nitrogen atoms. We also neglect the vibrational wall-relaxation, since we treat plasmas where the V-V and V-T processes dominate the wall relaxation. In the V-V and V-T processes, we consider only single-quantum transition processes. We assume that the total density of nitrogen molecules is constant owing to their small dissociation degree. As a result, the dissociated nitrogen atoms are assumed to associate into the v th vibrational level with probability R_v immediately after dissociation, which is assumed to be constant over v . Hence, we have the following master equation for the VDF of N₂ X¹Σ_g⁺ state:

$$\frac{dN_v}{dt} = N_e \sum_{w=0, \neq v}^M N_w C_{wv} - N_e N_v \sum_{w=0, \neq v}^M C_{vw} + N_{v-1} \sum_{w=0, \neq v}^{M-1} N_{w+1} Q_{v-1, v}^{w, w+1} + N_{v+1} \sum_{w=0, \neq v}^{M-1} N_w Q_{v+1, v}^{w, w+1} - N_v \left(\sum_{w=0, \neq v}^{M-1} N_{w+1} Q_{v, v+1}^{w+1, w} + \sum_{w=0, \neq v}^{M-1} N_w Q_{v, v-1}^{w, w+1} \right)$$

| Reactions | Process |
|--|---------|
| $N_2(X; v = 0 - 8) + e^- \leftrightarrow N_2(X; w = 0 - 8 \neq v) + e^-$ | e-V |
| $N_2(X; v) + N_2(X; w) \leftrightarrow N_2(X; v + 1) + N_2(X; w - 1)$ | V-V |
| $N_2(X; M) + N_2(X; w) \rightarrow 2N(2p^4S^o) + N_2(X; w - 1)$ | V-Diss |
| $N_2(X; v) + N_2(X) \leftrightarrow N_2(X; v - 1) + N_2(X)$ | V-T |

Table 3. List of collisions included in the master equation of VDF, eq. (38).

$$+ [N_2] (N_{v-1} P_{v-1,v} + N_{v+1} P_{v+1,v}) - N_v [N_2] (P_{v,v-1} + P_{v,v+1}) + R_v, \quad (38)$$

where N_v is the number density of the N₂ X state at the v th vibrationally excited level, C_{wv} is the rate coefficient of the electron impact vibrational excitation ($w < v$) or deexcitation ($w > v$) from level w to v , Q and P are the rate coefficients of V-V transfer and V-T relaxation, respectively, between the levels given by the following suffixes for N₂-N₂ collisions, and R_v is the rate of atomic nitrogen recombination into the v th level. The upper limit of the summation M is set at $v = 45$, which is considered to be the dissociation level of the nitrogen molecule, considered to be followed by instantaneous association into level v , which corresponds to the term R_v in eq. (38).

6.3 Reactions relevant to formation of excited species in the model

We include the electron-impact processes as in Table 4, and some of their reverse processes. To obtain the cross section of the reverse process, we apply the principle of detailed balance, which is known as the Klein-Rosseland equation formulated below:

$$\frac{\sigma_{pq}(\varepsilon')}{\sigma_{qp}(\varepsilon'')} = \frac{g_q}{g_p} \frac{\varepsilon''}{\varepsilon'}, \quad (39)$$

| Electron Impact Excitation | | |
|------------------------------|-------------------|-----------------------------|
| $e^- + N_2(X^1\Sigma_g^+)$ | \leftrightarrow | $e^- + N_2(A^3\Sigma_u^+)$ |
| $e^- + N_2(X^1\Sigma_g^+)$ | \leftrightarrow | $e^- + N_2(B^3\Pi_g)$ |
| $e^- + N_2(X^1\Sigma_g^+)$ | \leftrightarrow | $e^- + N_2(C^3\Pi_u)$ |
| $e^- + N_2(X^1\Sigma_g^+)$ | \leftrightarrow | $e^- + N_2(a'^1\Sigma_u^-)$ |
| $e^- + N_2(X^1\Sigma_g^+)$ | \leftrightarrow | $e^- + N_2(a^1\Pi_g)$ |
| Electron Impact Ionization | | |
| $e^- + N_2(X^1\Sigma_g^+)$ | \rightarrow | $e^- + e^- + N_2^+$ |
| Electron Impact Dissociation | | |
| $e^- + N_2(X^1\Sigma_g^+)$ | \rightarrow | $e^- + 2N(2p^4S^o)$ |
| Dissociative Recombination | | |
| $e^- + N_2^+$ | \rightarrow | $2N(^4S^o)$ |
| $e^- + N_4^+$ | \rightarrow | $2 N_2(X^1\Sigma_g^+)$ |

Table 4. List of electron collision processes included in term G in eq. (35).

where $\sigma_{pq}(\varepsilon')$ is the cross section for the electron impact reaction from level p to q with energy difference $\varepsilon_{pq} > 0$ for electron energy ε' , $\sigma_{qp}(\varepsilon'')$ is that of the reverse reaction with electron energy $\varepsilon'' = \varepsilon' + \varepsilon_{pq}$ and g_p is the statistical weight of state p .

We also take the atomic and molecular collision processes into account listed in Table 5. We also include one of their reverse processes, whose rate coefficient k_r is obtained from that of the forward reaction k_f and the equilibrium constant K_{eq} as

$$k_f/k_r = K_{eq}. \quad (40)$$

We calculate the equilibrium constant using the partition functions involved in the reactions.

| Chemical Reactions included in term G of eq. (35) | | |
|---|-------------------|--|
| $N_2(a' \ ^1\Sigma_u^-) + N_2(X \ ^1\Sigma_g^+)$ | \rightarrow | $N_2(B \ ^3\Pi_g) + N_2(X \ ^1\Sigma_g^+)$ |
| $N_2(C \ ^3\Pi_u) + N_2(X \ ^1\Sigma_g^+)$ | \rightarrow | $N_2(a' \ ^1\Sigma_u^-) + N_2(X \ ^1\Sigma_g^+)$ |
| $N_2(a \ ^1\Pi_g) + N_2(X \ ^1\Sigma_g^+)$ | \leftrightarrow | $N_2(a' \ ^1\Sigma_u^-) + N_2(X \ ^1\Sigma_g^+)$ |
| $N_2(B \ ^3\Pi_g) + N_2(X \ ^1\Sigma_g^+)$ | \rightarrow | $2N_2(X \ ^1\Sigma_g^+)$ |
| $N_2(A \ ^3\Sigma_u^+) + N_2(X \ ^1\Sigma_g^+)$ | \rightarrow | $2N_2(X \ ^1\Sigma_g^+)$ |
| $N_2(A \ ^3\Sigma_u^+) + N(2p \ ^4S^o)$ | \rightarrow | $N_2(X \ ^1\Sigma_g^+) + N(2p \ ^4S^o)$ |
| $N_2(A \ ^3\Sigma_u^+) + N_2(A \ ^3\Sigma_u^+)$ | \rightarrow | $N_2(B \ ^3\Pi_g) + N_2(X \ ^1\Sigma_g^+)$ |
| $N_2(A \ ^3\Sigma_u^+) + N_2(A \ ^3\Sigma_u^+)$ | \rightarrow | $N_2(C \ ^3\Pi_u) + N_2(X \ ^1\Sigma_g^+)$ |
| $N_2(a' \ ^1\Sigma_u^-) + N_2(X \ ^1\Sigma_g^+)$ | \rightarrow | $N_2^+ + N_2(X \ ^1\Sigma_g^+) + e^-$ |
| $N_2(a' \ ^1\Sigma_u^-) + N_2(a' \ ^1\Sigma_u^-)$ | \rightarrow | $2N_2^+ + 2e^-$ |
| $N_2(X \ ^1\Sigma_g^+, v \geq 6) + N_2(A \ ^3\Sigma_u^+)$ | \rightarrow | $N_2(B \ ^3\Pi_g) + N_2(X \ ^1\Sigma_g^+)$ |
| $N_2(B \ ^3\Pi_g) + N_2(X \ ^1\Sigma_g^+)$ | \rightarrow | $N_2(A \ ^3\Sigma_u^+) + N_2(X \ ^1\Sigma_g^+)$ |
| $2N(2p \ ^4S^o) + N(2p \ ^4S^o)$ | \rightarrow | $N_2(B \ ^3\Pi_g) + N(2p \ ^4S^o)$ |
| $N_2(a' \ ^1\Sigma_u^-) + N_2(A \ ^3\Sigma_u^+)$ | \rightarrow | $N_4^+ + e^-$ |
| $N_2(a' \ ^1\Sigma_u^-) + N_2(a' \ ^1\Sigma_u^-)$ | \rightarrow | $N_4^+ + e^-$ |

Table 5. List of atomic and molecular processes included in term G in eq. (35).

Some radiative decay processes of excited species are essential for the population kinetics due to large absolute value, which are summarized in Table 6. We must also include wall loss processes due to diffusion or thermal motion for several excited species, particularly for metastable states and ions. From the wall loss probability γ , we can calculate the wall loss frequency ν_w as follows:

$$\nu_w = \frac{\gamma v_{th}}{2R} \quad \text{for } \gamma \ll 1, \quad (41)$$

$$\nu_w = \left(\frac{2.405}{R} \right)^2 D \quad \text{for } \gamma \sim 1, \quad (42)$$

where R is the discharge tube radius, v_{th} is the thermal velocity of the particle considered, and D denotes the diffusion coefficient. For ionic species, we apply ambipolar diffusion coefficient. Table 7 shows the wall loss processes considered in the present model.

| Radiative transitions | Name of Transition |
|--|--|
| $N_2(B^3\Pi_g) \rightarrow N_2(A^3\Sigma_u^+) + h\nu$ | 1st Positive System |
| $N_2(C^3\Pi_u) \rightarrow N_2(B^3\Pi_g) + h\nu$ | 2nd Positive System |
| $N_2(a'^1\Sigma_u^-) \rightarrow N_2(a'^1\Sigma_u^-) + h\nu$ | Farlane Infrared System |
| $N_2(a'^1\Pi_g) \rightarrow N_2(X^1\Sigma_g^+) + h\nu$ | Lyman-Birge-Hopfield System |
| $N_2(a'^1\Sigma_u^-) \rightarrow N_2(X^1\Sigma_g^+) + h\nu$ | Ogawa-Tanaka-Wilkinson-Mulliken System |

Table 6. List of radiative transitions included in term G in eq. (35).

| Wall loss processes included in term G of eq. (35) | | | |
|--|---------------|----------------------|-------------------------------|
| $\gamma \ll 1$ [eq.(41)] | | | |
| $2N(2p^4S^o) + \text{wall}$ | \rightarrow | $N_2(X^1\Sigma_g^+)$ | $\gamma = 1.0 \times 10^{-4}$ |
| $N_2(a'^1\Sigma_u^-) + \text{wall}$ | \rightarrow | $N_2(X^1\Sigma_g^+)$ | $\gamma = 1.0 \times 10^{-2}$ |
| $\gamma \sim 1$ [eq.(42)] | | | |
| $N_2(A^3\Sigma_u^+) + \text{wall}$ | \rightarrow | $N_2(X^1\Sigma_g^+)$ | $\gamma = 1.0$ |
| $N_2(a'^1\Pi_g) + \text{wall}$ | \rightarrow | $N_2(X^1\Sigma_g^+)$ | $\gamma = 1.0$ |
| $N_2^+ + \text{wall}$ | \rightarrow | $N_2(X^1\Sigma_g^+)$ | $\gamma = 1.0$ |

Table 7. List of wall loss processes included in term G of eq. (35).

6.4 Numerical procedure

We calculate the number densities of the excited species depicted in Fig. 14. We solve eq. (35) for each species until we find that a steady state is accomplished for every state. The input parameters are the reduced electric field E/N , electron number density N_e , gas temperature T_g , and discharge pressure P . It should be remarked that the electron density is chosen as an input parameter, and consequently, the resultant ion density does not necessarily equal N_e . In order to maintain quasi-neutrality in the present calculation, we modify the value of P or T_g and repeat the algorithm in Fig. 14 until the quasi-neutral condition is fulfilled (Akatsuka et al., 2008; Ichikawa et al., 2010).

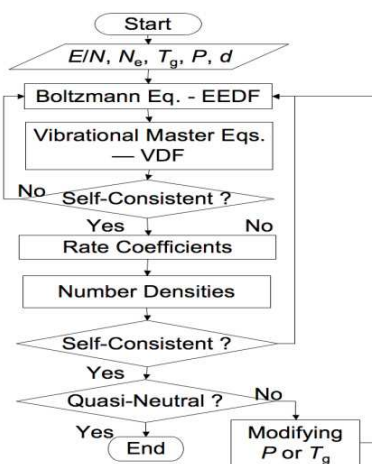


Fig. 14. Flow chart of the numerical procedure (Akatsuka et al., 2008; Ichikawa et al., 2010).

6.5 Numerical results and discussion

Figures 15(a) and 15(b) show the calculation results of EEPF and VDF of $N_2 X$, respectively. The calculations were run at $T_g = 1200$ K, $N_e = 5.0 \times 10^{11} \text{ cm}^{-3}$ and $T_e = 2.5 - 4.5$ eV. These parameters were chosen to correspond to our experimental results at $P = 1.0$ Torr and $z = 60$ mm obtained in the experimental apparatus shown in Fig. 3. It should be repeated that we choose a reduced electric field so that the electron mean energy $\langle \varepsilon \rangle$ equals $(3/2)kT_e$ when we compare the numerical calculation with the number densities obtained experimentally by OES measurement. Obviously, the EEPF is not like Maxwellian. It has a dip in the range from 2 to 3 eV owing to frequent consumption of electrons with this energy range due to inelastic collisions to make vibrationally excited molecules. Meanwhile, Fig. 15(b) shows that the VDF is also quite far from the Maxwellian distribution. The number density of the vibrational levels shows rapid decrease first, then moderate decrease, and rapid decrease again as the vibrational quantum number increases. This behaviour of the VDF of $N_2 X$ state has been frequently reported, and consequently, our model is also considered to be appropriate. If we can assume corona equilibrium of some excited states of N_2 molecule, for example, $N_2 C$ state, we can calculate the number density of the vibrational levels of the excited state that can be experimentally observed. This indicates that we can verify the appropriateness of the calculated VDF of the $N_2 X$ state as shown in Fig. 15(b).

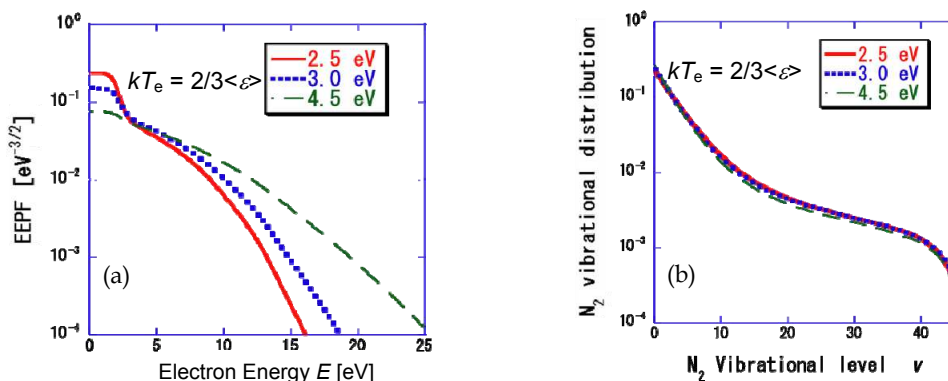


Fig. 15. (a) EEPF and (b) VDF of nitrogen plasma calculated numerically by the present scheme with pressure $P = 1$ Torr, $T_g = 1200$ K and $N_e = 5.0 \times 10^{11} \text{ cm}^{-3}$.

Another interesting result of this modelling is the identification of essential kinetic processes of population and depopulation of each excited state of N_2 molecule. Table 8 shows reaction rates of dominant population and depopulation processes for B and C state of nitrogen molecule, calculated for $T_e = 3.0$ eV, $N_e = 4.0 \times 10^{11} \text{ cm}^{-3}$, and $P = 1.0$ Torr (Akatsuka et al., 2008). When we examined the essential processes to populate and depopulate $N_2 B$ state and $N_2 C$ state, we found a marked difference between them. That is, the C state populates mainly by electron impact excitation from the $N_2 X$ state, the ground state of molecule, and depopulates mainly by radiative decay to the B state, i.e., by 2PS emission. It indicates that the C state is almost in the state of corona equilibrium. In the meanwhile, the B state populates mainly by intermolecular collision between $N_2 X$ ($v \geq 6$) and $N_2 A$ states, and depopulates by collisional quenching to $N_2 A$ state by the ground state molecule.

Consequently, the B state is quite far from the corona equilibrium. We should notice that the vibrational states of N₂ X is, indeed, essential to calculate the populations of excited states like B state, where the excitation through the intermolecular collisions plays an important role. Therefore, we must calculate the VDF together with the excitation kinetics of electronically excited states of N₂ molecule.

| Population Reaction | | Rate [cm ⁻³ s ⁻¹] |
|---------------------|--|--|
| C | N ₂ (X) + e ⁻ → N ₂ (C) + e ⁻ | 6.8 × 10 ¹⁷ |
| | N ₂ (A) + N ₂ (A) → N ₂ (C) + N ₂ (X) | 1.2 × 10 ¹⁷ |
| | Depopulation Reaction | Rate [cm ⁻³ s ⁻¹] |
| | N ₂ (C) → N ₂ (B) + hν | 8.0 × 10 ¹⁷ |
| Population Reaction | | Rate [cm ⁻³ s ⁻¹] |
| B | N ₂ (X, v ≥ 6) + N ₂ (A) → N ₂ (B) + N ₂ (X) | 1.84 × 10 ¹⁸ |
| | N ₂ (X) + e ⁻ → N ₂ (B) + e ⁻ | 1.23 × 10 ¹⁸ |
| | N ₂ (C) → N ₂ (B) + hν | 0.80 × 10 ¹⁸ |
| | N ₂ (A) + N ₂ (A) → N ₂ (B) + N ₂ (X) | 0.24 × 10 ¹⁸ |
| | N ₂ (a') + N ₂ (X) → N ₂ (B) + N ₂ (X) | 0.01 × 10 ¹⁸ |
| | Depopulation Reaction | Rate [cm ⁻³ s ⁻¹] |
| | N ₂ (B) + N ₂ (X) → N ₂ (A) + N ₂ (X) | 2.09 × 10 ¹⁸ |
| | N ₂ (B) → N ₂ (A) + hν | 1.89 × 10 ¹⁸ |
| | N ₂ (B) + N ₂ (X) → N ₂ (X) + N ₂ (X) | 0.14 × 10 ¹⁸ |

Table 8. Reaction rates of essential population and depopulation processes for B and C states of nitrogen molecule, calculated for $T_e = 3.0$ eV, $N_e = 4.0 \times 10^{11}$ cm⁻³, and $P = 1.0$ Torr.

This is also experimentally confirmed by the spectroscopic observation of vibrational levels of N₂ B and C states. If we assume the corona equilibrium of the excited states, we can calculate the vibrational distribution of the states from that of N₂ X state with the application of the Franck-Condon principle. Figures 16(a) and 16(b) show the comparison between the calculated and measured vibrational number densities of B ³Π_g (v = 7, 8, 9) state and those of C ³Π_u (v = 0 – 4) state, respectively, at $P = 1.0$ Torr and $z = 60$ mm measured with the

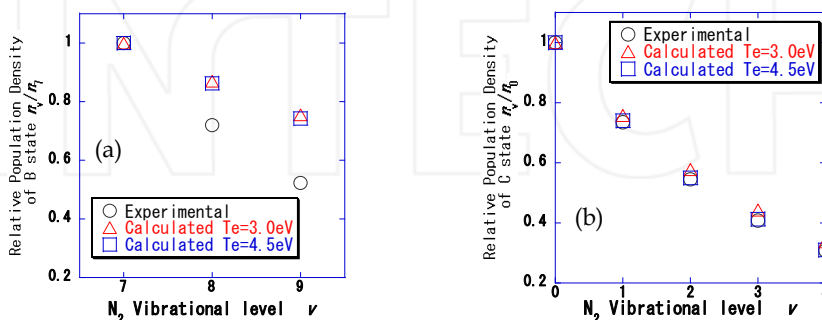


Fig. 16. Measured and calculated number densities of vibrational levels of N₂. (a) B ³Π_g v = 7, 8, and 9 and (b) C ³Π_u v = 0 – 4 (Sakamoto et al., 2007).

apparatus shown in Fig. 3. The agreement in the number densities observed by OES measurement with those calculated theoretically is excellent in $C^3\Pi_u$ ($v = 0 - 4$) state. On the other hand, it is found that of $B^3\Pi_g$ ($v = 7, 8, 9$) state does not agree with each other at all. One of the essential reasons for these findings lies in the respect that C state is in the corona equilibrium, while B state is not. Anyway, when we discuss the number densities of electronically excited states of N_2 in discharge plasmas, we should include the kinetics of vibrational levels as well as of population-depopulation mechanisms.

7. Conclusion

There still remain innovative and challenging applications about OES measurement of nitrogen plasma relevant to atomic and molecular processes. Following the introduction, section 2 introduced how to analyze 2PS spectrum with unresolved rotational structures, by which we can understand thermal structure of plasma processes.

Next in section 3, we introduced analysis of the 1PS spectrum. Although the procedure to analyze 1PS bands becomes far more complicated than 2PS bands, the basic strategy is the same as that of 2PS. We also demonstrated the resultant rotational temperature of 1PS is almost the same with that of 2PS for our microwave discharge nitrogen plasma. We should further examine its characteristics of vibrational non-equilibrium.

In chapter 4, we reviewed analysis of 1NS spectrum from N_2^+ ions. We also found that the rotational temperature of 1NS bands is much higher than that of 1PS or 2PS. We must further examine the reason why the 1NS bands of nitrogen show higher rotational temperature through atomic and molecular processes in the gas discharge.

In section 5, we demonstrated actinometry measurement of density of nitrogen atoms by subtracting the calculated 1PS spectrum from the one observed experimentally. Since lines from excited nitrogen atoms in the near-visible wavelength region severely overlap the 1PS band spectrum, it has been considered to be difficult to apply to nitrogen plasmas with low-dissociation degree. We overcame the problem and created another method to measure the number density of nitrogen atoms with inexpensive equipment with low-resolution.

In section 6, we introduced our simple modelling to analyze the excitation kinetics in the nitrogen plasma, which have been widely studied all over the world. This kind of modelling is essential to understand the spectroscopic characteristics of nitrogen plasmas, particularly the nonequilibrium kinetics of the vibrational levels.

We should not consider that nitrogen plasma is a commonplace industrial tool, but must scientifically respect its complicated excitation kinetics. Spectroscopic observation is one of the best experimental methods to understand it, simple and inexpensive. However, to do so, we must study its chemical kinetics after due consideration. We hope many researchers will become interested and take part in the study of this field.

8. Acknowledgment

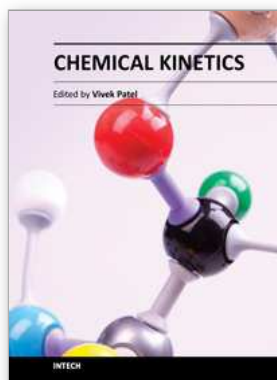
The author thanks Mr. S. Koike, Mr. H. Kobori, Mr. R. Toyoyoshi, Mr. K. Naoi, Mr. N. Kitamura, Mr. T. Ichiki, Mr. S. Kakizaka, Mr. Y. Ohno, Mr. Y. Ichikawa, Mr. J. Mizuochi, Mr. Y. Shimizu, Mr. Y. Kittaka, Mr. T. Shibata, Mr. W. Takai, Mr. K. Kuwano, Mr. H. Kawano and, particularly, Dr. T. Sakamoto for their cooperation in spectroscopic study or atomic-

molecular processes of plasmas. The author also thanks Prof. T. Yuji of University of Miyazaki, Prof. H. Matsuura, Dr. M. Matsuzaki and Mr. A. Nezu of Tokyo Institute of Technology for their helpful discussion. This study was partly supported by Grant-in-Aids for Scientific Research from the Japan Society for the Promotion of Science.

9. References

- Akatsuka, H.; Ichikawa, Y.; Sakamoto, T.; Shibata, T. & Matsuura, H. (2008). Population Kinetics and Number Densities of Excited Species in Low-Pressure Discharge Nitrogen Plasma, *Proceedings of The 6th EU-Japan Joint Symposium on Plasma Processing (EU-Japan JSPP)*, pp. 13-14, Okinawa Convention Centre, Okinawa, Japan, April 2008
- Akatsuka, H.; Kuwano, K.; Nezu, A. & Matsuura, H. (2010). Measurement of Nitrogen Dissociation Degree of Nitrogen Discharge Plasma by Actinometry Method with Subtraction of First Positive Band Spectrum; *Proceedings of the 63rd Gaseous Electronics Conference 2010 & 7th International Conference on Reactive Plasmas (GEC10/ICRP7)*, pp. 59-60, ISBN 978-4-86348-101-5, Paris, France, October 2010
- Bingel, W. A. (1967). Theorie der Molekülspektren, In: *Chemische Taschenbücher No. 2*, W. Foerst & H. Grunewald (Eds.) Verlag Chemie, ISBN 978-3-527-25017-2 Weinheim/Bergstr Germany [in German]
- Czerwiec, T.; Greer, F. & Graves, D. B. (2005). Nitrogen Dissociation in a Low Pressure Cylindrical ICP Discharge Studied by Actinometry and Mass Spectrometry. *J. Phys. D : Appl. Phys.*, Vol. 38, No. 24, (December 2005), pp. 4278-4289, ISSN 0022-3727
- D'Agostino, R.; Favia, P.; Kawai, Y.; Ikegami, H.; Sato, N & Arefi-Khonsari, F. (Eds.). (2008). *Advanced Plasma Technology*, Wiley-VCH, ISBN 978-3-527-40591-6, Weinheim, Germany
- Fridman, A. (2008). *Plasma Chemistry*, Cambridge University Press, ISBN-13 978-0-521-84735-3, New York, USA
- Guerra, V. & Loureiro J. (1997). Self-Consistent Electron and Heavy-Particle Kinetics in a Low-Pressure N₂-O₂ Glow Discharge. *Plasma Sources Sci. Technol.*, Vol. 6, No. 3, (August 1997), pp. 373-385, ISSN 0963-0252
- Guerra V.; Sá, P. A. & Loureiro J. (2004). Kinetic Modeling of Low-Pressure Nitrogen Discharges and Post-Discharges. *Eur. Phys. J. Appl. Phys.*, Vol. 28, No. 2, (November 2004), pp. 125-152, ISSN 1286-0042
- Hrachová, V.; Damiy, A.-M.; Kylián, O.; Kaňka A. & Legrand, J.-C. (2002). Behaviour of Glow and Microwave Discharges of Oxygen, In: *Advances in Plasma Physics Research*, F. Gerard, (Ed.), pp. 33-54, Nova Science Publishers, ISBN 1-59033-329-2, New York, USA
- Huang, X.-J.; Xin Y.; Yang, L.; Yuang, Q.-H. & Ning, Z.-U. (2008). Spectroscopic Study on Rotational and Vibrational Temperature of N₂ and N₂⁺ in Dual-Frequency Capacitively Coupled Plasma. *Phys. Plasmas*, Vol. 15, No. 11, (November 2008), pp. 113504-1-113504-6, ISSN 1070-664X
- Ichikawa, Y.; Sakamoto, T.; Nezu, A.; Matsuura, H. & Akatsuka, H. (2010). Actinometry Measurement of Dissociation Degrees of Nitrogen and Oxygen in N₂-O₂ Microwave Discharge Plasma. *Jpn. J. Appl. Phys.*, Vol. 49, No. 10, (October 2010), pp. 106101-1-106101-16, ISSN 1347-4065
- Kawano, H.; Nezu, A.; Matsuura, H. & Akatsuka, H. (2011). Estimation of Vibrational and Rotational Temperatures of N₂⁺ of Microwave Discharge Nitrogen Plasma by

- Optical Emission Spectroscopy Measurement. *The Papers of Technical Meeting on "Plasma Science and Technology"*, IEE Japan, Vol. PST-11, No. 2, pp. 15-18, [in Japanese]
- Kobori, S.; Koike, S.; Watanabe, S.; Matsuzaki M.; Matsuura, H. & Akatsuka, H. (2004). Dependence of Nitriding Degree of Ti Surface by Non-LTE Nitrogen Plasma on Various Plasma Parameters. *Thin Solid Films*, Vol. 457, No. 1, (June 2004), pp. 69-77, ISSN 0040-6090
- Koike, S.; Sakamoto, T.; Kobori, H.; Matsuura, H. & Akatsuka, H. (2004). Spectroscopic Study on Vibrational Nonequilibrium of a Microwave Discharge Nitrogen Plasma. *Jpn. J. Appl. Phys.*, Vol. 43, No. 8A, (August 2004), pp. 5550-5557, ISSN 1347-4065
- Kuwano, K.; Nezu, A.; Matsuura, H. & Akatsuka, H. (2009). Fundamental Study on Discharge Characteristics of Nitrogen-Rare Gas Microwave Plasma; *Proceedings of 6th Asia-Pacific International Symposium on the Basic and Application of Plasma Technology (APSPT 6)*, Minghsin University of Science and Technology, Hsinchu, ROC, December 2009 pp. 207-210
- Mizuochi, J.; Sakamoto, T.; Matsuura, H. & Akatsuka, H. (2010). Evaluation of Electron Energy Distribution Function in Microwave Discharge Plasmas by Spectroscopic Diagnostics with Collisional Radiative Model. *Jpn. J. Appl. Phys.*, Vol. 49, No. 3, (March 2010), pp. 036001-1-036001-14, ISSN 1347-4065
- Nunomura, S.; Kondo, M. & Akatsuka, H. (2006). Gas Temperature and Surface Heating in Plasma Enhanced Chemical-Vapour-Deposition. *Plasma Sources Sci. Technol.*, Vol. 15, No. 4, (November 2006), pp. 783-789, ISSN 0963-0252
- Ochkin, V. N. (2009). *Spectroscopy of Low Temperature Plasma*, WILEY-VCH, ISBN 978-3-527-40778-1, Weinheim, Germany
- Phillips, D. M. (1976). Determination of Gas Temperature from Unresolved Bands in the Spectrum from a Nitrogen Discharge. *J. Phys. D: Appl. Phys.*, Vol. 9, No. 3, (March 1976), pp. 507-521, ISSN 0022-3727
- Sakamoto, T.; Matsuura, H. & Akatsuka, H. (2006). Spectroscopic Study on Vibrational Distribution of N_2 C $^3\Pi$ and B $^3\Pi$ States in Microwave Nitrogen Discharge. *Jpn. J. Appl. Phys.*, Vol. 45, No. 10A, (October 2006), pp. 7905-7910, ISSN 1347-4065
- Sakamoto, T.; Matsuura, H. & Akatsuka, H. (2007). Spectroscopic Study on the Vibrational Populations of N_2 C $^3\Pi$ and B $^3\Pi$ States in a Microwave Nitrogen Discharge. *J. Appl. Phys.*, Vol. 101, No. 2, (February 2007), pp. 023307-1-023307-7, ISSN 0021-8979
- Shakhatov, V. A. & Lebedev, Yu. A. (2008). Kinetics of Excitation of N_2 (A $^3\Sigma_u^+$, v_A), N_2 (C $^3\Pi_u$, v_C), and N_2 (B $^3\Pi_g$, v_B) in Nitrogen Discharge Plasmas as Studied by Means of Emission Spectroscopy and Computer Simulation, *High Energy Chemistry*, Vol. 42, No. 3, (May 2008), pp. 170-204, ISSN 0018-1439
- Tatarova, E.; Dias, F. M.; Gordiets, B. & Ferreira, C. M. (2005). Molecular Dissociation in N_2 - H_2 Microwave Discharges. *Plasma Sources Sci. Technol.*, Vol. 14, No. 1, (February 2005), pp. 19-31, ISSN 0963-0252
- Yuji, T.; Suzuki, Y.; Yamawaki, T.; Sakaue, H. & Akatsuka, H. (2007). Experimental Study of Temperatures of Atmospheric-Pressure Nonequilibrium Ar/ N_2 Plasma Jets and Poly(ethylene terephthalate)-Surface Processing. *Jpn. J. Appl. Phys.*, Vol. 46, No. 2, (February 2007), pp. 795-798, ISSN 1347-4065
- Yuji, T.; Urayama, T.; Fujii, S.; Mungkung, N. & Akatsuka, H. (2008). Temperature Behavior of Atmospheric-Pressure Non-Equilibrium Microwave Discharge Plasma Jets for Poly(ethylene naphthalate)-Surface Processing. *Surface & Coatings Technology*, Vol. 202, No. 22-23, (August 2008), pp. 5289-5292, ISSN 0257-8972



Chemical Kinetics

Edited by Dr Vivek Patel

ISBN 978-953-51-0132-1

Hard cover, 344 pages

Publisher InTech

Published online 29, February, 2012

Published in print edition February, 2012

Chemical Kinetics relates to the rates of chemical reactions and factors such as concentration and temperature, which affects the rates of chemical reactions. Such studies are important in providing essential evidence as to the mechanisms of chemical processes. The book is designed to help the reader, particularly students and researchers of physical science, understand the chemical kinetics mechanics and chemical reactions. The selection of topics addressed and the examples, tables and graphs used to illustrate them are governed, to a large extent, by the fact that this book is aimed primarily at physical science (mainly chemistry) technologists. Undoubtedly, this book contains "must read" materials for students, engineers, and researchers working in the chemistry and chemical kinetics area. This book provides valuable insight into the mechanisms and chemical reactions. It is written in concise, self-explanatory and informative manner by a world class scientists in the field.

How to reference

In order to correctly reference this scholarly work, feel free to copy and paste the following:

Hiroshi Akatsuka (2012). Progresses in Experimental Study of N2 Plasma Diagnostics by Optical Emission Spectroscopy, Chemical Kinetics, Dr Vivek Patel (Ed.), ISBN: 978-953-51-0132-1, InTech, Available from: <http://www.intechopen.com/books/chemical-kinetics/progresses-in-experimental-study-of-n2-plasma-diagnostics-by-optical-emission-spectroscopy>

INTech

open science | open minds

InTech Europe

University Campus STeP Ri
Slavka Krautzeka 83/A
51000 Rijeka, Croatia
Phone: +385 (51) 770 447
Fax: +385 (51) 686 166
www.intechopen.com

InTech China

Unit 405, Office Block, Hotel Equatorial Shanghai
No.65, Yan An Road (West), Shanghai, 200040, China
中国上海市延安西路65号上海国际贵都大饭店办公楼405单元
Phone: +86-21-62489820
Fax: +86-21-62489821